Journal for ImmunoTherapy of Cancer

Targeting B7-H3 inhibition-induced activation of fatty acid synthesis boosts anti-B7-H3 immunotherapy in triple-negative breast cancer

Ying Jiang,[1] Zhiwen Qian,[2] Cenzhu Wang,[3] Danping Wu,[1] Lu Liu,[1] Xin Ning,[1] Yilan You,[2] Jie Mei ,[4] Xiaoqian Zhao,[5] Yan Zhang [1,2]

To cite: Jiang Y, Qian Z, Wang C, *et al*. Targeting B7-H3 inhibition-induced activation of fatty acid synthesis boosts anti-B7-H3 immunotherapy in triple-negative breast cancer. *Journal for ImmunoTherapy of Cancer* 2025;**13**:e010924. doi:10.1136/jitc-2024-010924

► Additional supplemental material is published online only. To view, please visit the journal online (https://doi.org/10.1136/jitc-2024-010924).

YJ, ZQ and CW contributed equally.

JM, XZ and YZ are joint senior authors.

Accepted 03 April 2025

Check for updates

© Author(s) (or their employer(s)) 2025. Re-use permitted under CC BY-NC. No commercial re-use. See rights and permissions. Published by BMJ Group.

For numbered affiliations see end of article.

Correspondence to
Dr Jie Mei;
meijie1996@njmu.edu.cn

Dr Xiaoqian Zhao;
snoppyy1980@163.com

Dr Yan Zhang;
fuyou2007@126.com

ABSTRACT

Background Triple-negative breast cancer (TNBC) is the most malignant breast cancer, highlighting the need for effective immunotherapeutic targets. The immune checkpoint molecule B7-H3 has recently gained attention as a promising therapeutic target due to its pivotal role in promoting tumorigenesis and cancer progression. However, the therapeutic impact of B7-H3 inhibitors (B7-H3i) remains unclear.

Methods Transcriptomic and metabolomic analyses were conducted to explore the underlying mechanisms of B7-H3 inhibition in TNBC. The therapeutic efficacy of the combined treatment strategy was substantiated through comprehensive phenotypic assays conducted in vitro and validated in vivo using animal models.

Results B7-H3 blockade induces a "primed for death" stress state in cancer cells, leading to distinct alterations in metabolic pathways. Specifically, B7-H3 knockdown activated the AKT signaling pathway and upregulated sterol regulatory element-binding protein 1 (SREBP1), which in turn elevated FASN expression. The simultaneous inhibition of both B7-H3 and FASN more effectively attenuated the malignant progression of TNBC.

Conclusions Our findings propose an "immune attack-metabolic compensation" dynamic model and suggest the feasibility of a dual-targeting strategy that concurrently inhibits both B7-H3 and FASN to enhance therapeutic efficacy in TNBC patients.

WHAT IS ALREADY KNOWN ON THIS TOPIC

⇒ Triple-negative breast cancer (TNBC) is a highly aggressive breast cancer subtype, characterized by limited therapeutic options and poor prognosis. Targeting B7-H3 holds promise for improving treatment outcomes in TNBC patients. Nevertheless, the molecular-level impact of targeting B7-H3 specifically in TNBC remains insufficiently studied.

WHAT THIS STUDY ADDS

⇒ This study not only elucidates the critical role of B7-H3 in the malignant progression of TNBC but also proposes viable therapeutic strategies to enhance the clinical efficacy of B7-H3i. In particular, we present the analysis of how B7-H3 inhibition reshapes the metabolic landscape of TNBC cells.

HOW THIS STUDY MIGHT AFFECT RESEARCH, PRACTICE OR POLICY

⇒ We introduce an innovative therapeutic approach by combining B7-H3i with the FASN inhibitors, significantly augmenting the anticancer response. This novel combinatorial strategy not only provides a potential avenue for more personalized and effective treatment options for TNBC patients but also holds promise for broader application in other malignancies.

BACKGROUND

Breast cancer (BC) remains the most prevalent malignancy among women, accounting for 31% of all female cancers according to recent data from the American Cancer Society.[1] It is also the second-leading cause of cancer-related deaths in women.[2] Among the subtypes, triple-negative BC (TNBC) represents 10%–20% of cases and is distinguished by the absence of estrogen receptor, progesterone receptor (PR), and human epidermal growth factor receptor 2 (HER2).[3] TNBC is typically more aggressive, with a high propensity for metastasis and recurrence, resulting in significantly worse prognosis compared with other BC subtypes.[4] Treatment options for TNBC are limited due to the lack of well-defined biomarkers,[5] underscoring the urgent need for effective therapeutic strategies.

Immunotherapy has emerged as a promising approach for TNBC. The US Food and Drug Administration (FDA) has approved several immune checkpoint inhibitors (ICIs) in combination with other therapies, providing new therapeutic avenues for TNBC.[6 7] In recent years, immune therapies centered around PD-L1/PD-1 inhibitors have significantly improved clinical outcomes in certain TNBC patients. However, the

J Immunother Cancer: first published as 10.1136/jitc-2024-010924 on 12 April 2025. Downloaded from http://jitc.bmj.com/ on May 20, 2025 at Department GEZ-LTA Erasmushogeschool . Protected by copyright, including for uses related to text and data mining, AI training, and similar technologies.

objective response rate to PD-L1/PD-1 inhibitors remains around 20%, leaving a substantial portion of patients with suboptimal therapeutic responses.[8] Building on these challenges, our previous research pioneered an innovative TNBC subtyping strategy based on the expression of B7-H3 and PD-L1, revealing that B7-H3 is highly expressed when PD-L1 expression is low.[9] B7-H3 is highly expressed on tumor cells and tumor-associated vasculature, while exhibiting minimal presence in normal tissues. This distinct and selective expression pattern contributes to the development of an immune evasion phenotype, which in turn promotes cancer cell proliferation, metastasis, and drug resistance.[10] Notably, T lymphocytes, a cardinal component of antitumor immunity, are markedly suppressed in the presence of elevated B7-H3 expression.[11–14] Given the widespread overexpression of B7-H3 in tumors and its association with an immunosuppressive microenvironment, various B7-H3-targeted therapies—including monoclonal antibodies (mAbs), antibody-drug conjugates, and CAR-T cell therapies—are undergoing clinical evaluation and have demonstrated promising preliminary efficacy.[15–21] However, the molecular effects of B7-H3 inhibition in TNBC remain largely unexplored.

In this study, we conducted transcriptomic and metabolomic analyses of TNBC cells following B7-H3 knockdown, revealing that B7-H3 suppression activated FASN-mediated de novo fatty acid (FA) synthesis. Notably, the dual inhibition of B7-H3 and FASN significantly potentiated anticancer effects, as evidenced by both in vitro assays and in vivo models. These results highlight a novel therapeutic strategy that integrates B7-H3 and FASN inhibition, offering a promising avenue for improving treatment outcomes in TNBC.

METHODS

Bioinformatics analysis

The expressions of B7-H3 in normal, BC and -TNBC tissues were investigated in The Cancer Genome Atlas (TCGA) database through the UALCAN database (https://ualcan.path.uab.edu/) while the expression comparison was analyzed by the Wilcoxon test. The survival of B7-H3 and FASN was explored through the KM Plotter database (https://kmplot.com/analysis/), which was analyzed by the log-rank test. The enrichment analysis was performed by the "clusterProfiler", "org.Hs.eg.db", "enrichplot," and "ggplot2" R packages. The correlation analysis was conducted by the Spearman correlation analysis and was presented via the "ggplot2", "ggpubr", "ggExtra" R packages.

Single-cell RNA-seq data acquisition and analysis

Single-cell RNA sequencing was conducted by Shanghai Genechem Co., using the Illumina HiSeq XTen platform. Data processing, including sample demultiplexing, barcode assignment, and gene count generation for each cell, was performed using Cell Ranger V.3.0.2. For cell-type annotation, the R package "singleR" was used, referencing the Human Primary Cell Atlas, Blueprint Encode Data, and Immune Cell Expression Data. Uniform Manifold Approximation and Projection (UMAP) was used for dimensional reduction. Cells were classified into major cell types, including epithelial cells, immune cells, and stromal cells, based on canonical marker gene expression. For immune checkpoint expression analysis, B7-H3 expression was overlaid onto the UMAP plot, showing its distribution across different cell types within the tumor immune microenvironment. Expression levels were visualized with a color gradient to depict variation in gene expression, where yellow to purple indicates low to high expression levels, respectively.

Multiplexed immunohistochemistry and histochemistry staining

A paraffin-embedded tissue microarray (TMA) (catalog HBreD180Bc01-1) was obtained from Outdo BioTech (Shanghai, China). The primary antibodies used for immunofluorescence staining were: FASN (dilution 1:100, CST, catalog 3180) and B7-H3 (dilution 1:200, CST, catalog 14058).

Cell culture

The human breast epithelial cell line MCF-10A (catalog KGG3103-1) and TNBC cell lines MDA-MB-231 (catalog KGG3220-1) and BT549 (catalog KGG3221-1) were procured from KeyGEN Biotech (Nanjing, China). All human cell lines were authenticated via short tandem repeat (STR) analysis to confirm their identity. The cells were cultured in their respective recommended media, supplemented with 10% fetal bovine serum (FBS) and 1% penicillin-streptomycin, and maintained at 37°C in a humidified incubator containing 5% CO_2. Small interfering RNA (siRNA) was designed and synthesized by KeyGEN Biotech. Transient transfections were performed using Lipofectamine 3000 (ThermoFisher, catalog L3000015) at a final concentration of 100 nM.

Proliferation assays

Pretreated cells were resuspended and seeded into 96-well plates for CCK-8 assays. Cell proliferation was quantified by measuring the absorbance at 450 nm. Additionally, cells were evenly seeded into six-well plates and cultured for 1 week in a standard cell culture incubator. Colonies were subsequently fixed with paraformaldehyde (Solarbio, catalog P1110) and stained using crystal violet dye (Solarbio, catalog G1061). Colony formation was quantified using ImageJ software for both counting and documentation.

Migration and invasion assay

The Transwell assay is divided into two parts: the determination of migratory capacity (without the addition of Matrigel (Corning) in the chamber and the determination of invasive capacity (with the addition of Matrigel in the chamber). Pretreated cells were seeded in FBS-free medium into the upper chambers, while the lower chambers received medium supplemented with 10% FBS.

J Immunother Cancer: first published as 10.1136/jitc-2024-010924 on 12 April 2025. Downloaded from http://jitc.bmj.com/ on May 20, 2025 at Department GEZ-LTA Erasmushogeschool . Protected by copyright, including for uses related to text and data mining, AI training, and similar technologies.

After 48 hours of incubation, the cells that had migrated or invaded to the bottom surface of the membrane were fixed with paraformaldehyde and stained using crystal violet dye. The stained cells were then visualized and quantified.

Flow cytometry

The TNBC cells were harvested using 0.25% trypsin without EDTA and subjected to dual staining with the Annexin V-APC/7-AAD Cell Apoptosis Detection Kit (KeyGEN, catalog KGA1106-50). Apoptosis was assessed using a CytoFLEX flow cytometer.

Immunofluorescence analysis

Cells subjected to various treatments were washed twice with PBS and fixed with 4% paraformaldehyde at room temperature for 15 min. After fixation, cells were permeabilized using 0.1% Triton X-100 (Solarbio, catalog T8200). Blocking was performed with 10% goat serum for 30 min, followed by an overnight incubation with primary antibodies at 4°C. The primary antibody used was SREBP1 (1:400 dilution, Proteintech, catalog 66875-1-Ig). The next day, cells were incubated with fluorescently labeled secondary antibodies at room temperature. Nuclei were counterstained with DAPI (1:1000 dilution, Beyotime, catalog C1002), and cells were visualized using a confocal microscope (Nikon A1+, Japan).

RNA extraction and real-time quantitative PCR

Total RNA was extracted from cells using RNA-easy Isolation Reagent (Vazyme, catalog R701-01), following the manufacturer's protocol. cDNA was synthesized using the HiScript II Q RT SuperMix (Vazyme, catalog R222-01). Real-time quantitative PCR was then performed with ChamQ Universal SYBR qPCR Master Mix (Vazyme, catalog Q321-02), using β-actin as the normalization control. The following primer sequences were used: B7-H3: (forward) 5'- GGGCTGTCTGTCTGTCTCAT-3' and (reverse) 5'-TTTCTCCAGCACACGAAAGC-3'; FASN: (forward) 5'-AAGGACCTGTCTAGGTTTGATGC-3' and (reverse) 5'-TGGCTTCATAGGTGACTTCCA-3'; β-actin: (forward) 5'-GCAGAAGGAGATCACTGCCCT-3' and (reverse) 5'-GCTGATCCACATCTGCTGGAA-3'.

Western blot

Cells were harvested and homogenized on ice using RIPA buffer (Solarbio, catalog R0020) supplemented with PMSF (Solarbio, catalog P0100) and phosphatase inhibitors (Abcam, ab201113). The protein concentration in the supernatant was determined using a BCA assay (Vazyme, catalog E112-01). Equal amounts of protein were separated on 8%–12% SDS-PAGE gels (Vazyme, catalog E302-01, catalog E303-01, catalog E304-01) and subsequently transferred to polyvinylidene fluoride (PVDF) membranes (Millipore, catalog IPVH00010). Membranes were blocked with NcmBlot blocking buffer (NCM Biotech, catalog P30500) and incubated overnight with primary antibodies: FASN (1:1000 dilution, Abcam, catalog ab128856), SREBP1 (1:1000 dilution, Proteintech, catalog 66875-1-Ig), B7-H3 (1:1000 dilution, Abcam, catalog ab134161), p-AKT (1:1000 dilution, CST, catalog 4060), AKT (1:1000 dilution, CST, catalog 4691), p-mTOR (1:1000 dilution, CST, catalog 5536), mTOR (1:1000 dilution, CST, catalog 2983), β-actin (1:1000 dilution, Affinity Biosciences, catalog AF7018). The next day, membranes were incubated with HRP-conjugated secondary antibodies. Specific protein bands were visualized using the SuperPico ECL Chemiluminescence Kit (Vazyme, catalog E422-01) and imaged using the ChemiDoc XRS+system (Biorad, USA). Protein expression levels were normalized to β-actin.

RNA-sequencing analysis

Six samples, including three biological replicates from both the control group (si-NC) and the treatment group (si-B7-H3), underwent RNA sequencing. Illumina's second-generation high-throughput sequencing platform was used with a PE150 sequencing strategy. After quality control, clean read pairs were obtained. Alignment and transcript assembly analyses were performed using STAR and Cufflinks software, followed by quantitative analysis of all genes. The criteria for differential gene screening were set at $p<0.05$. Plant transcription factors were identified based on the Plant Transcription Factor Database 4.0 (http://planttfdb.cbi.pku.edu.cn/); animal transcription factors were identified using AnimalTFDB 3.0 (http://bioinfo.life.hust.edu.cn/AnimalTFDB/).

Metabolome analysis

Raw Liquid Chromatography-Tandem Mass Spectrometry (LC-MS/MS) data files were processed using the XCMS package for peak detection, alignment, and retention time correction of each metabolite. The "SVR" method was employed to correct peak areas, and peaks with missing rates exceeding 50% across samples were filtered out. Data were normalized using unit variance scaling before performing hierarchical clustering analysis. Orthogonal partial least squares discriminant analysis (OPLS-DA) was performed using the the OPLSR. Anal function from the MetaboAnalystR package in R. Differential metabolites were further screened based on the variable importance in projection (VIP) scores from the OPLS-DA model, combined with univariate analysis P-values. Metabolites with VIP scores greater than 1.0 and P-values < 0.05 were considered significantly different between groups.

Dual-Glo luciferase experiment

HEK293T cells were co-transfected with either the pGL3-FASN promoter MUT or pGL3-FASN promoter WT constructs, along with pcDNA3.1-NC or pcDNA3.1-OE and the pRL-TK Renilla luciferase vector, using KeygenMAX 3000 (Keygen, catalog KGA9705-1.5). 48 hours after transfection, firefly luciferase activity was measured by adding Dual-Glo Luciferase Reagent. After the initial reading, Dual-Glo Stop & Glo Reagent was added to measure Renilla luciferase activity. Firefly luciferase activity was

J Immunother Cancer: first published as 10.1136/jitc-2024-010924 on 12 April 2025. Downloaded from http://jitc.bmj.com/ on May 20, 2025 at Department GEZ-LTA Erasmushogeschool . Protected by copyright, including for uses related to text and data mining, AI training, and similar technologies.

normalized to Renilla luciferase activity to account for transfection efficiency.

Animal models

We used female BALB/c mice aged 5–6 weeks, purchased from the Shanghai Laboratory Animal Center. A suspension of cultured 4T1 BC cells (concentration of 1×10^7 cells/mL) was injected subcutaneously into the right axilla of mice at a volume of 0.1 mL per mouse. Tumor diameters were measured using a caliper, and when the tumor volume reached approximately 100 mm^3, mice were randomly divided into six groups: control, anti-B7-H3, anti-FASN, anti-B7-H3+anti FASN, anti-PD-L1, and anti-B7-H3+anti FASN+anti-PD-L1, with each group consisting of five mice. Treatment was initiated at this stage, and therapeutic agents were administered according to the assigned groups. These agents included the B7-H3 mAb (BioXCell, Catalog BE0124), the FASN inhibitor (MCE, HY-120394), and the PD-L1 mAb (BioXCell, Catalog BE0101). The B7-H3 mAb was intraperitoneally given at a dosage of 160 µg twice weekly, and the PD-L1 mAb was intraperitoneally given at a dosage of 200 µg twice weekly. Concurrently, the FASN inhibitor was orally administered at a dosage of 30 mg/kg once daily. This treatment regimen was sustained for a duration of 2 weeks to allow for a comprehensive assessment of the therapeutic effects. The antitumor effects were dynamically observed by regularly measuring tumor sizes. At the end of the experiment, mice were euthanized using carbon dioxide (Euthanex Chamber). Tumors were then extracted from the unconscious animals, and their weights were recorded. The excised tumor tissues were subjected to WB analysis and immunofluorescence staining. ImageJ software was used for quantitative analysis of fluorescence.

Statistical analysis

Statistical analyses and figure presentations were conducted using R language V.4.3 and GraphPad Prism V.9.5. Group differences were assessed using the Student's t-test or Wilcoxon for two groups, while one-way analysis of variance with Tukey's multiple-comparison test or the Kruskal-Wallis test with multiple comparisons was used for multiple groups. Prognostic values of categorical variables were assessed via the log-rank test. A $p<0.05$ was considered statistically significant for all analyses.

RESULTS

Overexpression of B7-H3 in TNBC and its clinical relevance

We initially delineated the expression of B7-H3 in BC. Analysis of the TCGA database indicated that B7-H3 is significantly overexpressed in BC tissues (figure 1A). Subsequently, single-cell sequencing was employed to further elucidate the expression patterns of B7-H3 within BC. This analysis revealed that epithelial and stromal cells were the primary cell types expressing B7-H3, with the former being the predominant cell type undergoing malignant transformation in BC and the latter playing a pivotal role in shaping the tumor environment (TME) (figure 1B). Notably, tumor cells, cancer-associated fibroblasts (CAFs), and myeloid cells were found to highly express B7-H3 (online supplemental figure 1A). CAFs are ubiquitous in the TME across various cancer types, exerting crucial effects on tumor progression and drug resistance through diverse mechanisms.[22] Myeloid cells are a crucial group of immune system components comprising macrophages, dendritic cells, monocytes, and granulocytes.[23] This observation aligns with a previous study that reported B7-H3 enrichment specifically in tumor-associated macrophages of TNBC patients.[24] Consequently, we explored the correlation between B7-H3 expression and tumor-infiltrating immune cells using data from TCGA. Our analysis demonstrated that high expression of B7-H3 is significantly associated with the formation of an immunosuppressive TME (online supplemental figure 1B–E). Given that TNBC is the most challenging subtype of BC to treat, these findings prompted us to further explore the expression profile and functional role of B7-H3 specifically in TNBC.

Compared with normal breast tissues, B7-H3 exhibits markedly elevated expression levels in TNBC (figure 1C). The Kaplan-Meier plotter online database analysis demonstrated that high B7-H3 expression is closely associated with reduced overall survival (OS) and relapse-free survival (RFS) in TNBC patients (figure 1D). Subsequently, we employed multiplex immunofluorescence staining on TMAs to further investigate protein expression patterns. figure 1E,F presents representative images illustrating B7-H3 expression in both cancerous and adjacent non-cancerous tissues. Statistical analysis results from TNBC microarray tumors (n=150) and adjacent non-cancerous tissues (n=30) revealed that B7-H3 expression was markedly higher in TNBC tissues (figure 1G). Moreover, Western Blot confirmed the elevated expression of B7-H3 in TNBC cells relative to non-cancerous breast epithelial cells (figure 1H,I). Collectively, these data suggested that B7-H3 is markedly overexpressed in TNBC and is linked to adverse clinical outcomes.

B7-H3 knockdown suppressed the malignant phenotypes of TNBC cells

Expression analysis, correlation analysis with immune cells, and survival analysis have established the pivotal role of B7-H3 in TNBC. Moving forward, our primary focus is on investigating the impact of B7-H3 on TNBC. To assess the response of TNBC to B7-H3 knockdown, we conducted a series of functional assays in TNBC cell lines. As shown in figure 2A, siRNA-B7-H3-1 was identified as the most effective in reducing B7-H3 expression levels. Western blot analysis further confirmed that siRNA-B7-H3-1 induced a significant reduction in protein levels (figure 2B,C). We selected this sequence for subsequent functional studies investigating cellular phenotypic changes. CCK-8 and colony formation assays revealed that B7-H3 silencing significantly diminishes the proliferative capacity of TNBC cells (figure 2D,E,G). Furthermore,

J Immunother Cancer: first published as 10.1136/jitc-2024-010924 on 12 April 2025. Downloaded from http://jitc.bmj.com/ on May 20, 2025 at Department GEZ-LTA Erasmushogeschool . Protected by copyright, including for uses related to text and data mining, AI training, and similar technologies.

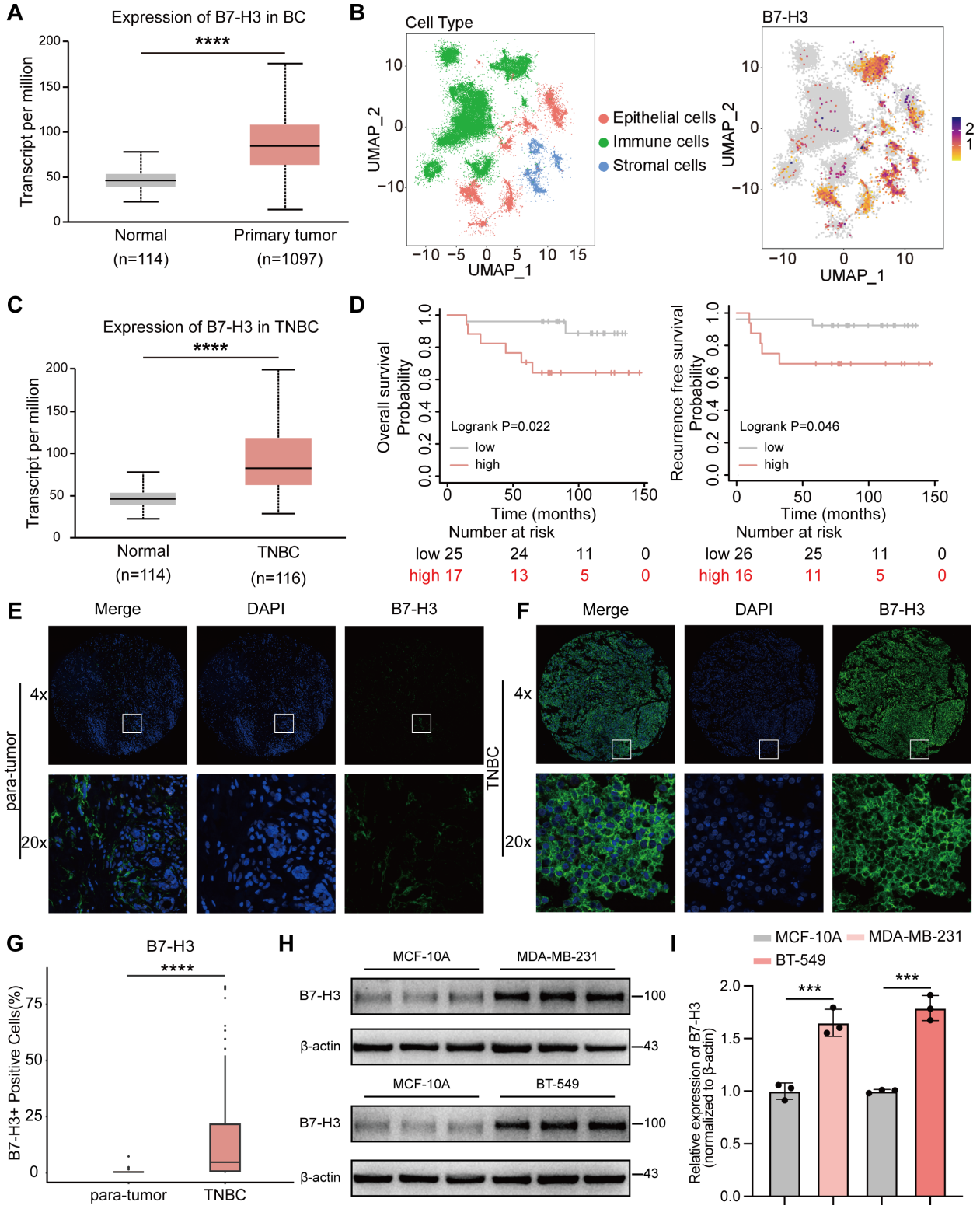

Figure 1 B7-H3 is highly expressed in TNBC. (A) B7-H3 is highly expressed in BC tissues. Significance was calculated with the Wilcoxon test. (B) Single-cell RNA sequencing (scRNA-seq) analysis of 10 BC patients revealed the distribution of different cell types within the BC TIME and the correlation between B7-H3 expression and scRNA-seq distribution. (C) B7-H3 is highly expressed in TNBC tissues. Significance was calculated with the Wilcoxon test. (D) Kaplan-Meier plotter analysis showed that high B7-H3 expression is associated with poor outcomes in TNBC patients. (E, F) Representative images of B7-H3 immunohistochemical staining in TNBC and adjacent non-cancerous tissues from tissue microarrays. (G) Statistical analysis of the proportion of B7-H3-positive cells in TNBC versus adjacent tissues. (H, I) Western blot analysis showed that B7-H3 expression is significantly higher in TNBC cells than in non-cancerous breast epithelial cells. Significance was calculated using the Student's t-test. ***p<0.001, ****p<0.0001. BC, breast cancer; TIME, tumor immune microenvironment; TNBC, triple-negative breast cancer.

J Immunother Cancer: first published as 10.1136/jitc-2024-010924 on 12 April 2025. Downloaded from http://jitc.bmj.com/ on May 20, 2025 at Department GEZ-LTA Erasmushogeschool . Protected by copyright, including for uses related to text and data mining, AI training, and similar technologies.

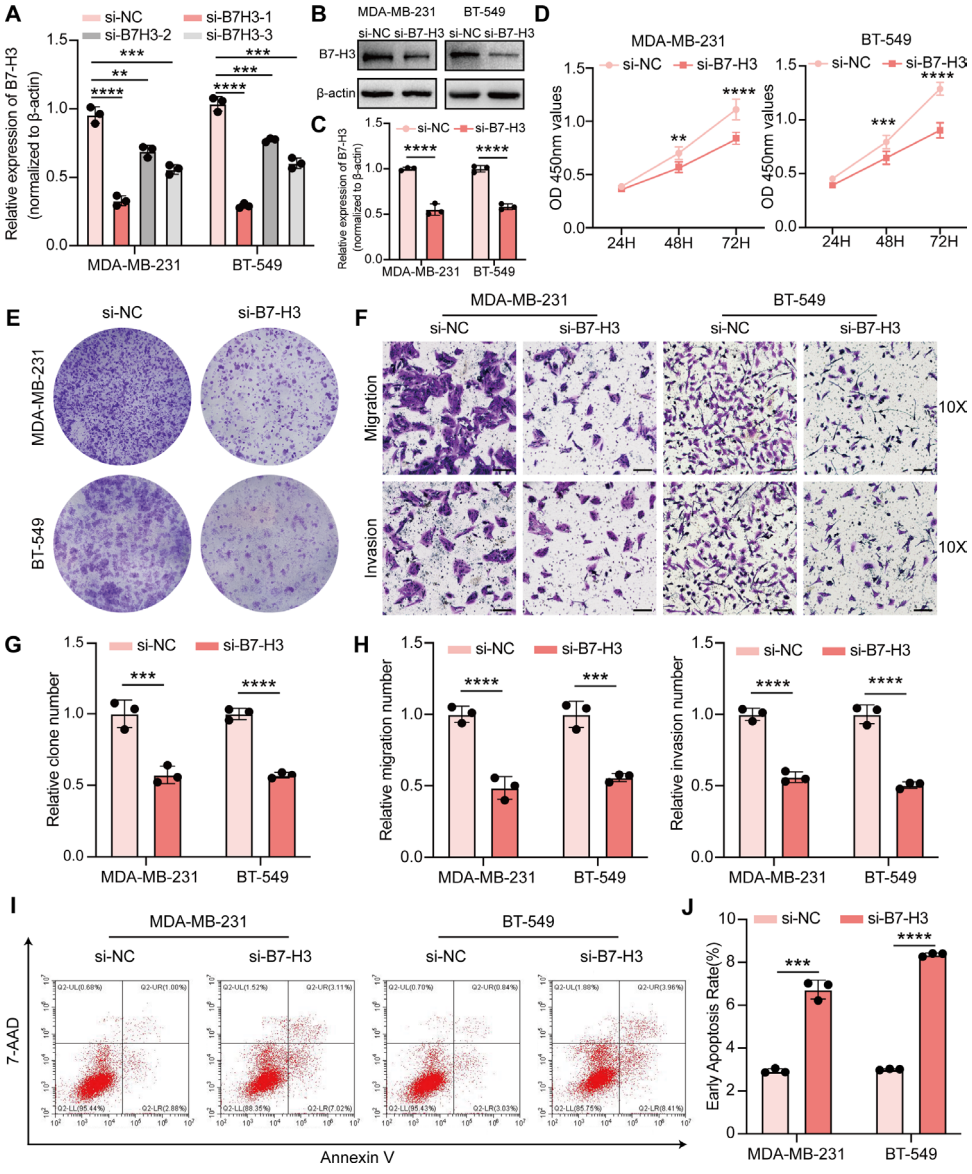

Figure 2 Biological functions of B7-H3 in TNBC cells. (A–C) Transfection efficiency of B7-H3 knockdown in TNBC cells. (D) B7-H3 knockdown suppressed TNBC cell proliferation as measured by the CCK-8 assay. (E, G) B7-H3 knockdown reduced colony formation capacity in TNBC cells. (F, H) B7-H3 knockdown impaired TNBC cell motility via transwell assay. Scale bars: 50 µm. (I, J) Downregulation of B7-H3 induced early apoptosis in TNBC cells. Data are presented as mean±SD (n=3). Significance was calculated using the Student's t-test. **p<0.01, ***p<0.001, ****p<0.0001. TNBC, triple-negative breast cancer.

Transwell migration and invasion assays demonstrated a striking reduction in the number of migrating and invading TNBC cells in the si-B7-H3 group compared with the si-NC group (figure 2F,H). This underscores the inhibitory effect of B7-H3 downregulation on TNBC cell motility. Complementing these observations, we discovered that the downregulation of B7-H3 significantly increased the early apoptotic rate among TNBC cells (figure 2I,J). Collectively, these findings underscore the pivotal role of B7-H3 in fostering the malignant traits of TNBC cells.

Metabolic expression profiling of TNBC cells following B7-H3 knockdown

The high expression of B7-H3 in TNBC and its critical role in promoting malignant progression support the use of anti-B7-H3 therapies in TNBC treatment. To further investigate the molecular effects of B7-H3 inhibition in TNBC, we performed transcriptomic sequencing on B7-H3-knockdown TNBC cells and control groups. Sequencing data underwent rigorous quality control (online supplemental figure 2A), and after quantifying gene expression, statistical analyses were conducted to identify genes with significant differential expression between the groups (online supplemental figure 2B,C). Then, we employed multiple enrichment analysis techniques to interrogate the RNA-seq data and uncover the processes altered by B7-H3 knockdown. Gene Ontology enrichment analysis highlighted dysregulated genes involved in metabolic remodeling (figure 3A,B). Gene Set Enrichment Analysis identified the top two metabolic

J Immunother Cancer: first published as 10.1136/jitc-2024-010924 on 12 April 2025. Downloaded from http://jitc.bmj.com/ on May 20, 2025 at Department GEZ-LTA Erasmushogeschool . Protected by copyright, including for uses related to text and data mining, AI training, and similar technologies.

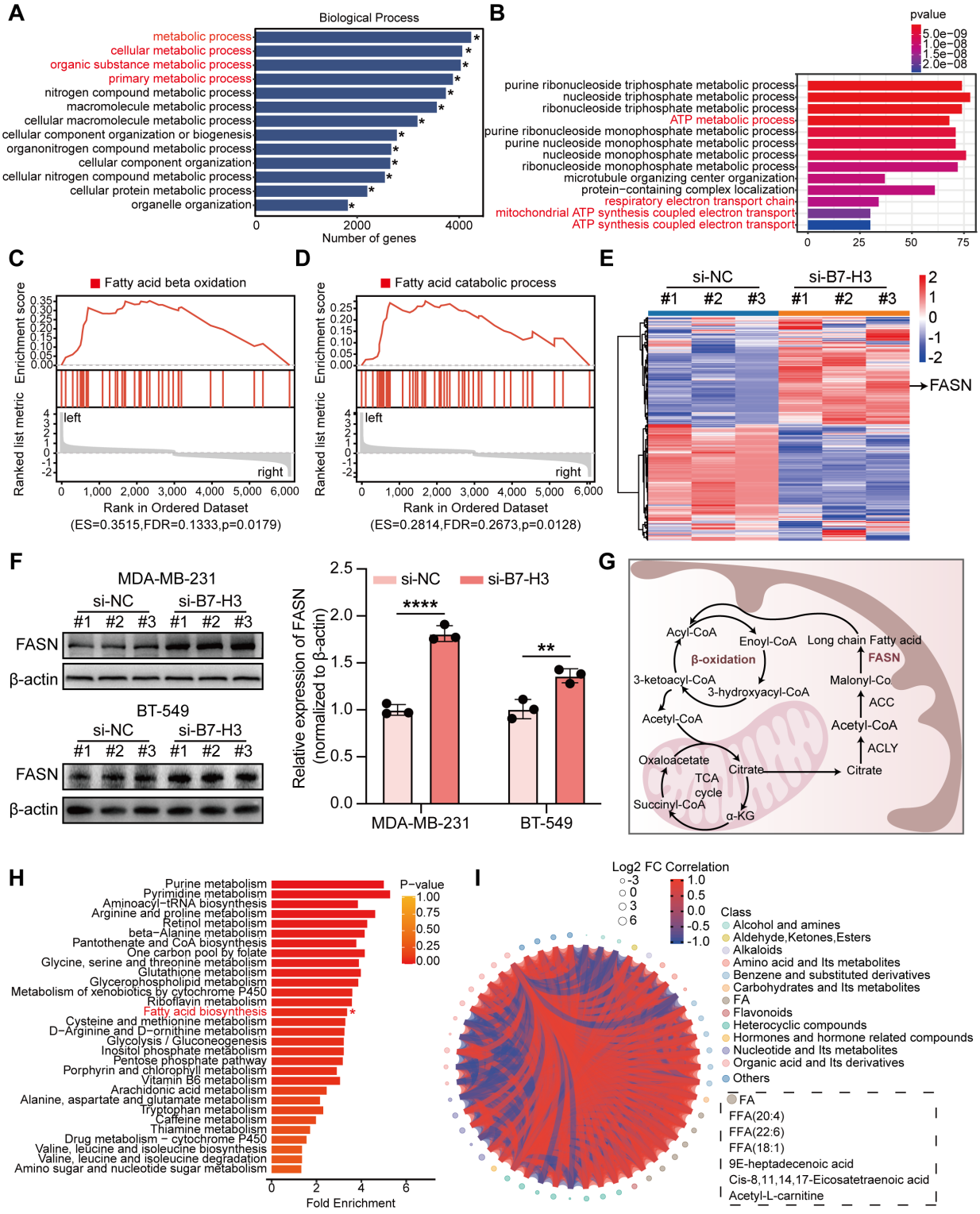

Figure 3 Transcriptional and metabolomic profiling in B7-H3 knockdown TNBC cells. (A, B) GO enrichment analysis of differentially expressed genes related to biological processes. (C, D) GSEA plots illustrated significant enrichment of fatty acid beta-oxidation and fatty acid catabolic processes in the ranked gene dataset. (E) Heat map of the differentially expressed genes between si-NC and si-B7-H3 cells (n=3). (F) Western blot analysis showed that B7-H3 knockdown leads to an increase in FASN protein levels. (G) Schematic representation of metabolic enzymes and processes altered after B7-H3 knockdown in MDA-MB-231 cells. (H) MSEA illustrates the fold enrichment of various metabolic pathways, highlighting significant changes in metabolic activities. (I) Chord diagram displaying differentially expressed metabolites and their classifications. The different colors represent various metabolite classes, while the lines indicate Pearson correlation coefficients between metabolites, with red lines indicating positive correlations and blue lines indicating negative correlations. Fatty acid metabolic products are highlighted. Statistical significance was calculated with Student's t-test. *p<0.05, **p<0.01, ****p<0.0001. MSEA, metabolite set enrichment analysis; TNBC, triple-negative breast cancer.

J Immunother Cancer: first published as 10.1136/jitc-2024-010924 on 12 April 2025. Downloaded from http://jitc.bmj.com/ on May 20, 2025 at Department GEZ-LTA Erasmushogeschool . Protected by copyright, including for uses related to text and data mining, AI training, and similar technologies.

pathways ranked by p-value, with FA β-oxidation showing a significant association (figure 3C,D), underscoring the impact of B7-H3 silencing on the regulation of FA metabolism. Therefore, we explored the key genes driving these metabolic alterations. The heatmap visualizes the distribution of differentially expressed genes (figure 3E). Notably, the transcriptomic analysis revealed a marked upregulation of the key FA metabolism enzyme FASN in the B7-H3 knockdown group. Validation through Western Blot confirmed the elevated expression of FASN, consistent with the RNA-seq data (figure 3F). By integrating the insights from transcriptomic sequencing, we visually depicted the crosstalk between FASN-driven FA synthesis, FA β-oxidation, and ATP generation through the TCA cycle (figure 3G).

We conducted untargeted metabolomics analyses to validate these transcriptomic findings. Differential analysis integrating Variable Importance in Projection (VIP; VIP>1) scores from the OPLS-DA model and p values ($p<0.05$) identified 259 significantly upregulated and 66 downregulated metabolites. Comparison of metabolite fold changes between groups revealed that among the top 20 metabolites (15 upregulated and 5 downregulated), three were significantly upregulated lipid metabolism products (online supplemental figure 3A,B). Metabolite set enrichment analysis highlighted FA biosynthesis as a significantly impacted pathway (figure 3H). A chord diagram of differential metabolites showcased the top 50 metabolites with the highest VIP scores, including 6 positively correlated FA metabolism products with consistent abundance changes, further reinforcing the activation of FA metabolic pathways (figure 3I). These findings collectively suggest that B7-H3 knockdown leads to increased FA synthesis mediated by FASN, accompanied by crosstalk between enhanced FA β-oxidation and the activation of the mitochondrial TCA cycle. Literature searches suggest that both FA synthesis and β-oxidation may coexist and synergize to meet the heightened metabolic demands of tumor cells.[25] Based on these results, we hypothesize that B7-H3 silencing triggers compensatory upregulation of FA metabolic pathways, enabling tumor cells to counteract apoptosis and sustain survival. Although highly specific inhibitors of FA oxidation are currently unavailable, targeting FASN as a key enzyme in FA synthesis represents a promising therapeutic approach,[26] warranting further functional studies to explore its role in TNBC.

FASN silencing suppressed malignant behaviors in TNBC cells

Despite FASN's recognized importance in cancer biology, the specific expression characteristics and functional roles of FASN in TNBC remain inadequately understood and warrant further investigation. Our analysis of TCGA revealed a negative correlation between FASN expression and Gamma-delta (γδ) T cells (online supplemental figure 4A). γδ T cells exhibit unique antigen recognition capabilities and robust cytotoxicity.[27] Clinical responses to cancer immunotherapies involving ICIs appear to require the presence of γδ T cells capable of recognizing tumor neoantigens,[28] highlighting a potential interplay between FASN expression and immunotherapy efficacy in TNBC. Multiplex immunohistochemistry on tumor microarrays illustrated a representative image of FASN expression in both cancerous and adjacent non-cancerous tissues (figure 4A). Compared with adjacent non-cancerous tissues, FASN was highly expressed in tumor tissues (online supplemental figure 4B). Analysis of the Kaplan-Meier plotter online database revealed that higher FASN expression is associated with worse OS and RFS in TNBC patients (figure 4B). Subsequently, we conducted functional validation assays in TNBC cells to further substantiate these findings. The knockdown efficiency of FASN was validated at both the RNA and protein levels (online supplemental figure 4C,D). Studies have demonstrated that FASN knockdown significantly inhibits the clonogenic ability of TNBC cells (figure 4C,E). Notably, the downregulation of FASN markedly reduces the migratory and invasive capacities of TNBC cells (figure 4D,F). Furthermore, FASN depletion enhanced early apoptosis in TNBC cells, as demonstrated by flow cytometry analysis (figure 4G,H). These findings collectively underscore the critical role of FASN in driving TNBC aggressiveness and survival, positioning it as a promising therapeutic target.

B7-H3 knockdown enhanced the expression of FASN by upregulating SREBP1

In light of the oncogenic role of FASN and the amplified FASN overexpression triggered by B7-H3 silencing, we sought to elucidate the mechanisms responsible for the dysregulated activation of FASN. Given that B7-H3 silencing upregulates FASN mRNA levels, we hypothesized that this phenomenon might involve alterations in the expression of transcription factors governing FASN transcription. Consequently, we conducted a comprehensive analysis of transcriptomic profiles to investigate this possibility. We visualized the distribution of transcription factor families to gain insights into their activation profiles. Figure 5A illustrates the top 10 transcription factor families influenced in the B7-H3 knockdown group. Building on this foundation, we proceeded to use the JASPAR database to predict potential transcription factors that could be responsible for the activation of FASN. By selecting the top 12 transcription factors based on their track scores and intersecting them with differentially expressed transcription factors from the RNA-seq data, we identified SREBP1 as a key candidate of interest (figure 5B). Correlation analysis demonstrated a strong positive association between SREBP1 and FASN (figure 5C). To validate the functional role of SREBP1, we next examined whether it exerts transcriptional activation on FASN and whether this activity is enhanced following B7-H3 knockdown. The dual-luciferase assay results revealed a marked increase in luciferase activity in cells transfected with the wild-type FASN promoter construct, compared with the mutant construct where the SREBP1 binding site was altered, thus confirming the transcriptional activation role of SREBP1 on FASN (figure 5D).

J Immunother Cancer: first published as 10.1136/jitc-2024-010924 on 12 April 2025. Downloaded from http://jitc.bmj.com/ on May 20, 2025 at Department GEZ-LTA Erasmushogeschool . Protected by copyright, including for uses related to text and data mining, AI training, and similar technologies.

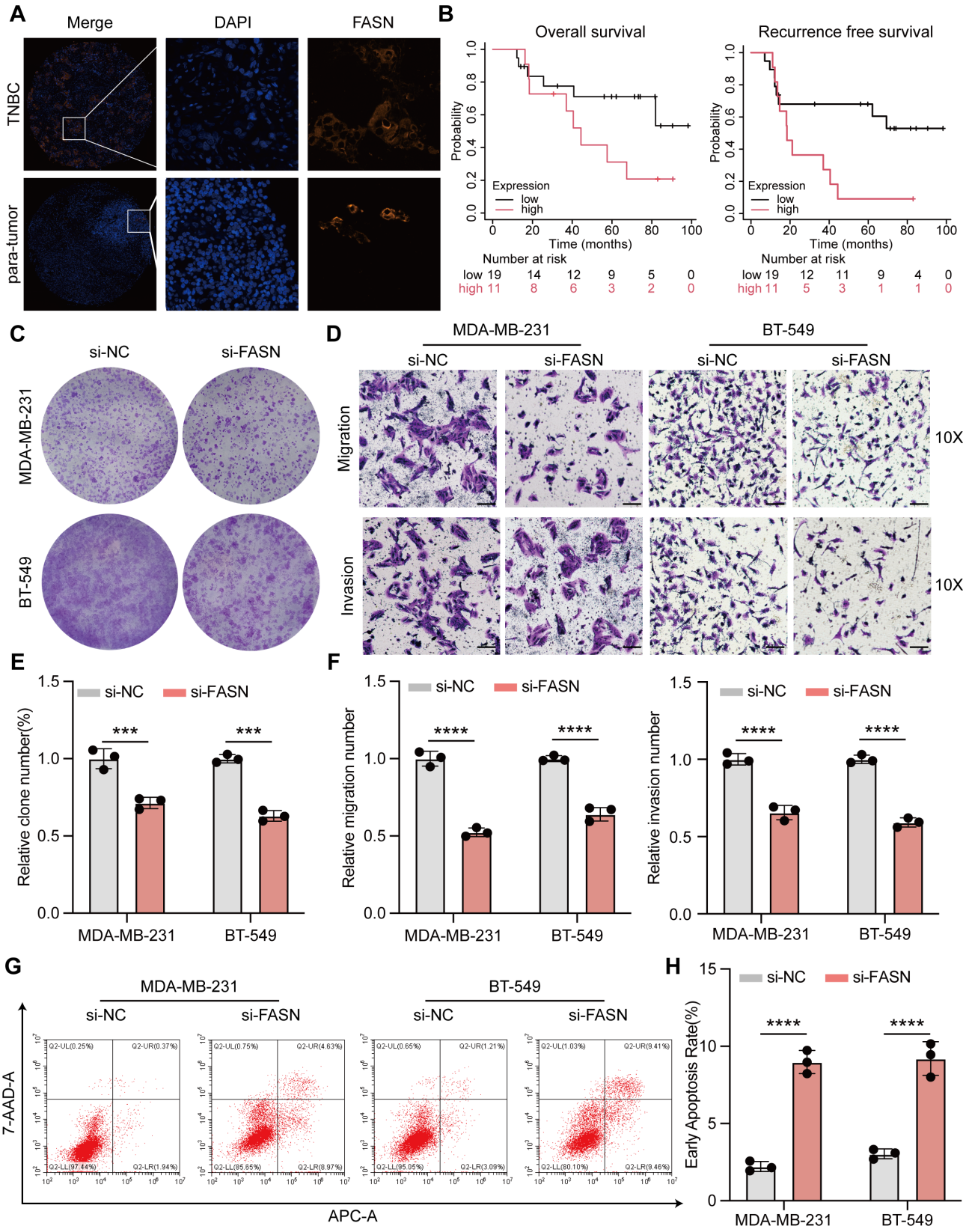

Figure 4 FASN affects the progression of TNBC cells. (A) Representative immunohistochemical staining images showing FASN expression in TNBC and adjacent non-cancerous tissues from tissue microarrays. (B) Kaplan-Meier Plotter analysis demonstrated that elevated FASN expression is linked to poorer prognosis in TNBC patients. (C, E) Knockdown of FASN reduced colony formation ability in TNBC cells. (D, F) Knockdown of FASN diminished TNBC cell motility, as shown by the transwell assay. Scale bars: 50 µm. (G, H) FASN downregulation triggered early apoptosis in TNBC cells. Data presented as mean±SD (n=3). Significance was calculated using the Student's t-test. ***p<0.001, ****p<0.0001. TNBC, triple-negative breast cancer.

J Immunother Cancer: first published as 10.1136/jitc-2024-010924 on 12 April 2025. Downloaded from http://jitc.bmj.com/ on May 20, 2025 at Department GEZ-LTA Erasmushogeschool . Protected by copyright, including for uses related to text and data mining, AI training, and similar technologies.

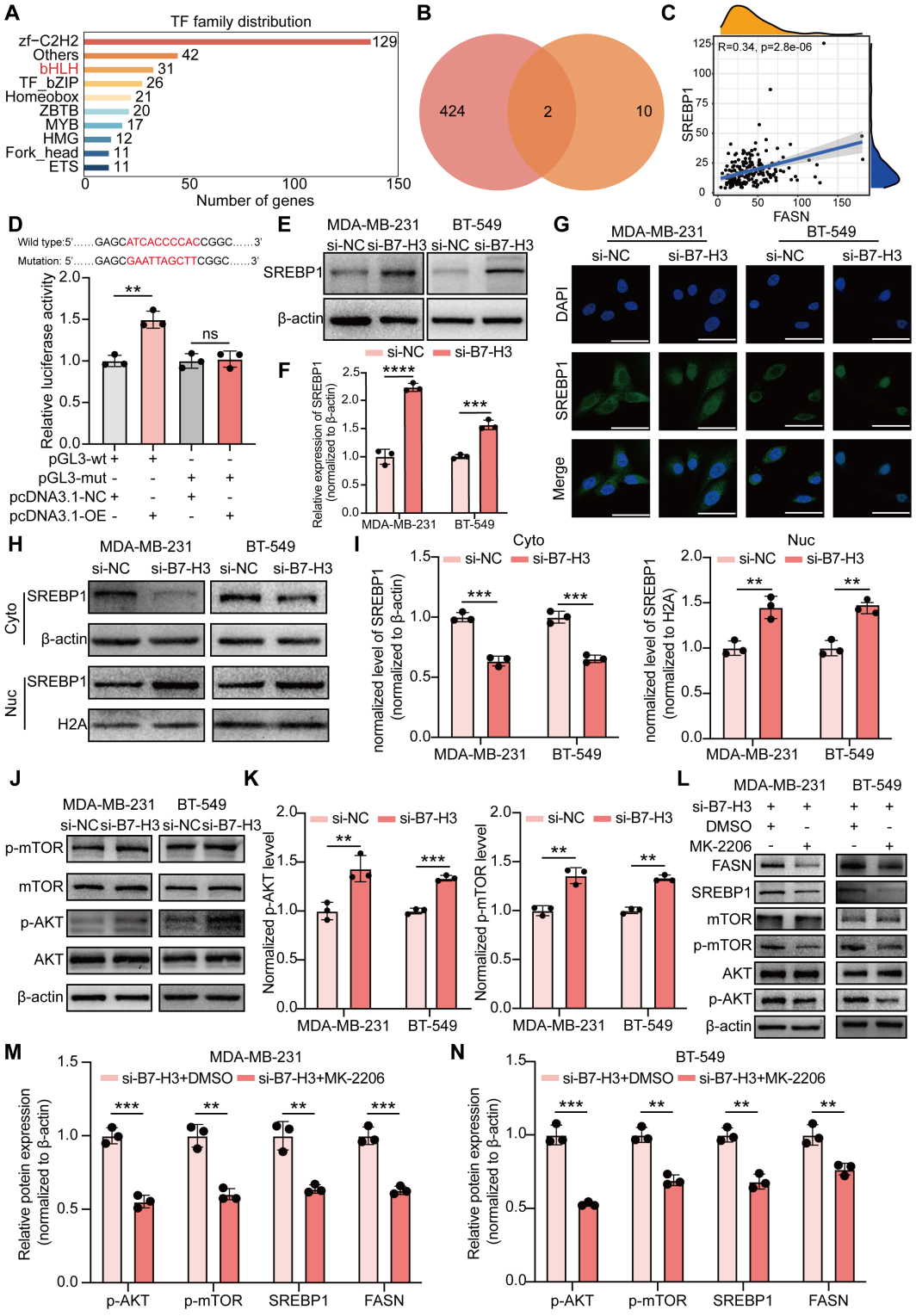

Figure 5 B7-H3 knockdown regulates FASN via the AKT pathway. (A) Visualization of TF family distribution by comparing all differentially expressed genes from transcriptomic data using BLAST against transcription factor databases. (B) Venn diagram showing candidate transcription factors selected from the JASPAR database and transcriptomic data. (C) Correlation between SREBP1 and FASN expression in TNBC. (D) The wild-type FASN promoter construct (pGL3-wt) exhibited significantly increased luciferase activity when cells were transfected with the pcDNA3.1 vector containing the SREBP1 gene. (E, F) B7-H3 knockdown upregulated SREBP1 expression. (G) Immunofluorescence assay showing nuclear translocation of SREBP1 following B7-H3 knockdown. Scale bars: 50 µm. (H, I) Western blot analysis confirmed the nuclear translocation of SREBP1 after B7-H3 knockdown. (J, K) Western blot analysis showed that protein levels of the Akt-mTOR signaling pathway were elevated in the si-B7-H3 group. (L–N) Western blot analysis demonstrating that inhibition of the Akt pathway suppressed the activation of both SREBP1 and FASN. Data are presented as mean±SD (n=3). Significance was calculated using the Student's t-test. ns: non-significance, **p<0.01, ***p<0.001, ****p<0.0001.

J Immunother Cancer: first published as 10.1136/jitc-2024-010924 on 12 April 2025. Downloaded from http://jitc.bmj.com/ on May 20, 2025 at Department GEZ-LTA Erasmushogeschool . Protected by copyright, including for uses related to text and data mining, AI training, and similar technologies.

Additionally, Western blot analysis validated the increased activation of SREBP1 in the context of B7-H3 knockdown (figure 5E,F). Nuclear-cytoplasmic fractionation and immunofluorescence assays further demonstrated that B7-H3 knockdown increased nuclear SREBP1 expression and promoted its translocation from the cytoplasm to the nucleus (figure 5G–I). These findings indicated that the activation of FASN might be mediated by the transcription factor SREBP1. To elucidate the mechanisms underlying the aberrant activation of SREBP1 and FASN, a deeper exploration of dysregulated pathways following B7-H3 silencing is warranted. Given the well-established link between the Akt signaling pathway and lipid metabolism,[29 30] we have focused our research on the Akt pathway. Western blot analysis confirmed significant activation of the Akt signaling pathway on B7-H3 knockdown (figure 5J,K). Rescue experiments showed that inhibition of the Akt pathway suppressed the activation of both SREBP1 and FASN (figure 5L–N). These results established that B7-H3 knockdown upregulated SREBP1 expression by activating the Akt pathway, which subsequently promoted the transcriptional activation of FASN.

FASN modulation augments the inhibitory impact of B7-H3 knockdown on cancer cells

The data presented above substantiated the activation of FASN subsequent to B7-H3 inhibition, and this activation may partially offset the tumor-suppressive effects of B7-H3 inhibition. To address this potential limitation, the primary focus of this section was to investigate whether the combined knockdown of B7-H3 and FASN could yield enhanced anti-tumor effects in TNBC cells. qPCR and Western blot analyses confirmed comparable knockdown efficiencies in both single-gene and dual-gene knockdown groups (figure 6A–C). Notably, in vitro proliferation assays demonstrated that dual knockdown of FASN and B7-H3 significantly suppressed TNBC cell proliferation compared with single-gene targeting (figure 6D,E). Furthermore, transwell migration and invasion assays revealed a striking attenuation of both migratory and invasive capacities in TNBC cells on combinatorial knockdown (figure 6F–I). Consistently, apoptosis assays demonstrated that the combined gene knockdown led to a higher rate of early-stage apoptosis in cancer cells (figure 6J–M). In conclusion, the co-silencing of B7-H3 and FASN elicited the most potent therapeutic effects.

Modulation of FASN enhances the anticancer effect of B7-H3 inhibition in vivo

To evaluate the efficacy of the dual therapeutic approach in vivo, we developed a mouse model of TNBC using the 4T1 cell line (figure 7A). On completion of the treatment, we first assessed the physiological parameters of the mice, confirming that cardiac, hepatic, and renal functions were normal across all treatment groups (online supplemental figure 5A–D). Additionally, no significant weight loss was observed in the treated groups compared with the untreated group, underscoring the tolerability of the treatments (online supplemental figure 5E). We confirmed the expression of B7-H3 and FASN in the 4T1 cells, as well as the inhibitory effects of the corresponding antibody and inhibitor (online supplemental figure 6A,B). Tumor volume growth curves and tumor weight analysis revealed that both anti-B7-H3 and anti-FASN monotherapies exhibited notable tumor-inhibitory effects, while the combination treatment produced a synergistic enhancement of these effects (figure 7B,C). Furthermore, protein extracted from tumor tissues not only supported but also extended the in vitro findings, revealing that B7-H3 inhibition leads to increased FASN expression, as evidenced by Western Blot analysis (figure 7D,E). Additionally, Oil Red O staining revealed the accumulation of lipid droplets within tumor cells specifically in the group treated with anti-B7-H3 (online supplemental figure 6C–F). HE staining further confirmed extensive necrosis of tumor cells in the group subjected to the combined treatment regimen (figure 7F). Moreover, immunofluorescent TUNEL staining and quantitative analysis demonstrated that the combination treatment significantly increased tumor cell apoptosis (figure 7G,H). Consistent with this, immunofluorescent analysis for CD8 revealed that higher levels of $CD8^+$ T cells were detected in the group receiving the combination treatment (figure 7I,J). As key "end effectors" of cancer immunity, the recruitment and activation of $CD8^+$ T cells are critical for eliciting effective antitumor immune responses.[31]

In 2020, the FDA approved the combination of the anti-PD-1 therapy pembrolizumab with nab-paclitaxel as a first-line treatment for metastatic TNBC.[32 33] In this context, we further investigated and validated the sensitizing effect of a combination therapy targeting B7-H3 and FASN on anti-PD-L1 therapy (figure 7K). Tumor volume growth curves and tumor weight analysis unequivocally demonstrated that the combination therapy significantly enhanced the effects of PD-L1 therapy (figure 7L,M, (online supplemental figure 6G-H). In line with these findings, HE staining demonstrated that the combination therapy, when administered alongside an anti-PD-L1 mAb, induced a more pronounced disruption in the overall architecture of the tumor tissue, characterized by extensive necrosis and apoptosis of tumor cells (figure 7N). TUNEL staining confirmed that this combined treatment, when used with anti-PD-L1 mAb, led to a significantly higher rate of apoptosis (figure 7O). Moreover, IHC analysis for $CD8^+$ T cells showed that, compared with anti-PD-L1 monotherapy, the combination therapy substantially increased the infiltration of $CD8^+$ T cells (figure 7P, online supplemental figure 6I).

Together, these findings suggest two key implications. First, for TNBC patients eligible for anti-B7-H3 therapy, experiments both in vitro and in vivo consistently demonstrated that targeting FASN enhances the tumor-inhibitory effects of anti-B7-H3 therapy. Second, this combination therapy significantly improves the efficacy of anti-PD-L1 therapy, and triple therapy may further enhance the overall

J Immunother Cancer: first published as 10.1136/jitc-2024-010924 on 12 April 2025. Downloaded from http://jitc.bmj.com/ on May 20, 2025 at Department GEZ-LTA Erasmushogeschool . Protected by copyright, including for uses related to text and data mining, AI training, and similar technologies.

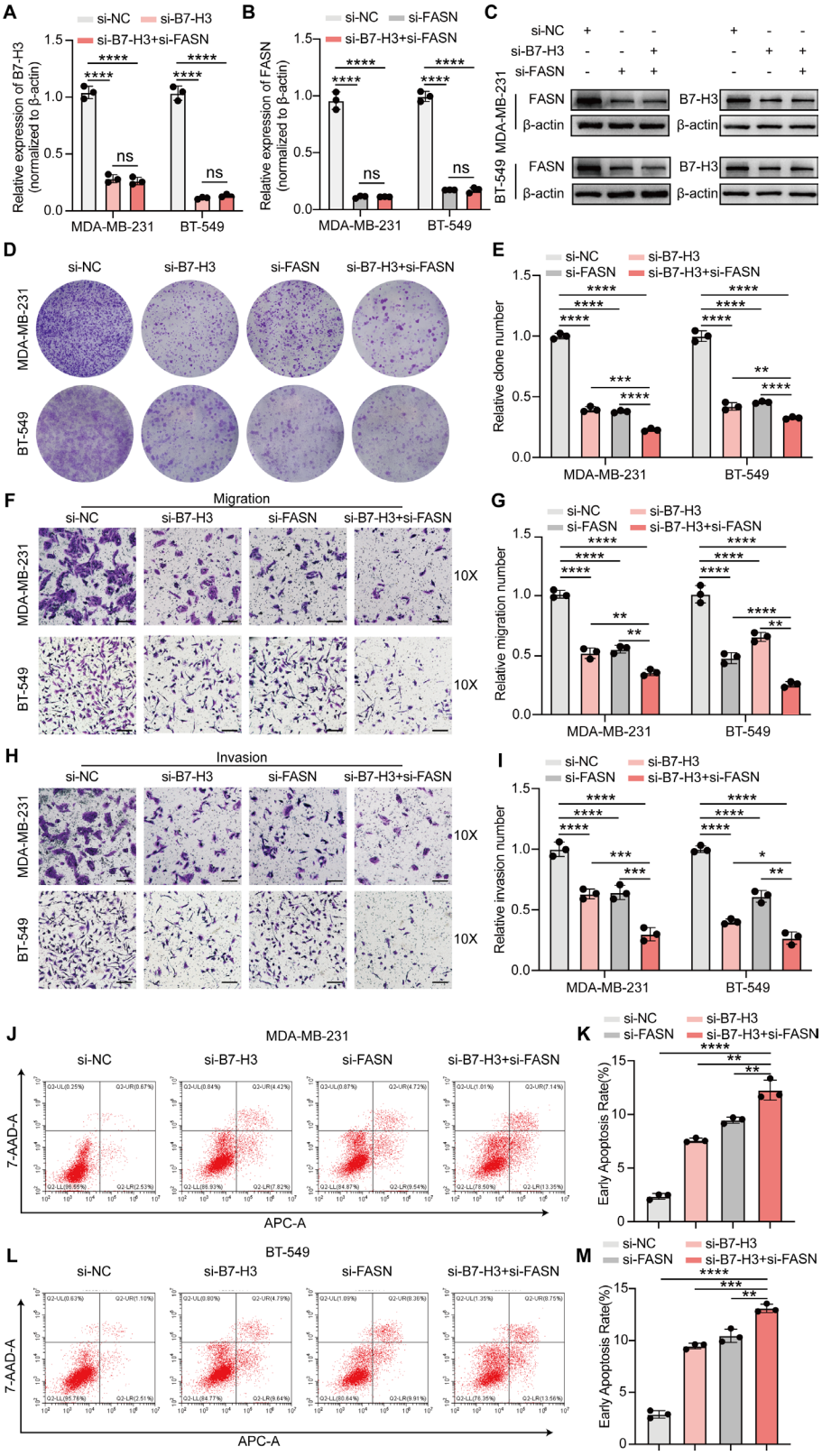

Figure 6 Combined knockdown of B7-H3 and FASN more effectively suppresses TNBC cell growth. (A–C) Quantitative PCR and Western blot analyses confirmed the knockdown of B7-H3 and FASN at both mRNA and protein levels in MDA-MB-231 and BT-549 cells. (D, E) Combined knockdown of B7-H3 and FASN significantly inhibited colony formation capacity in TNBC cells. (F, G) Co-silencing of B7-H3 and FASN more effectively reduced TNBC cell migration. Scale bars: 50 µm. (H–I) Combined knockdown further suppressed the invasive ability of TNBC cells. Scale bars: 50 µm. (J–M) Co-knockdown of B7-H3 and FASN promoted early apoptosis in TNBC cells more significantly. Data presented as mean±SD (n=3). Statistical significance was calculated with one-way ANOVA with Tukey's multiple-comparison test. ns: not significant, *p<0.05, ** p<0.01, ***p<0.001, ****p<0.0001. ANOVA, analysis of variance; TNBC, triple-negative breast cancer.

J Immunother Cancer: first published as 10.1136/jitc-2024-010924 on 12 April 2025. Downloaded from http://jitc.bmj.com/ on May 20, 2025 at Department GEZ-LTA Erasmushogeschool . Protected by copyright, including for uses related to text and data mining, AI training, and similar technologies.

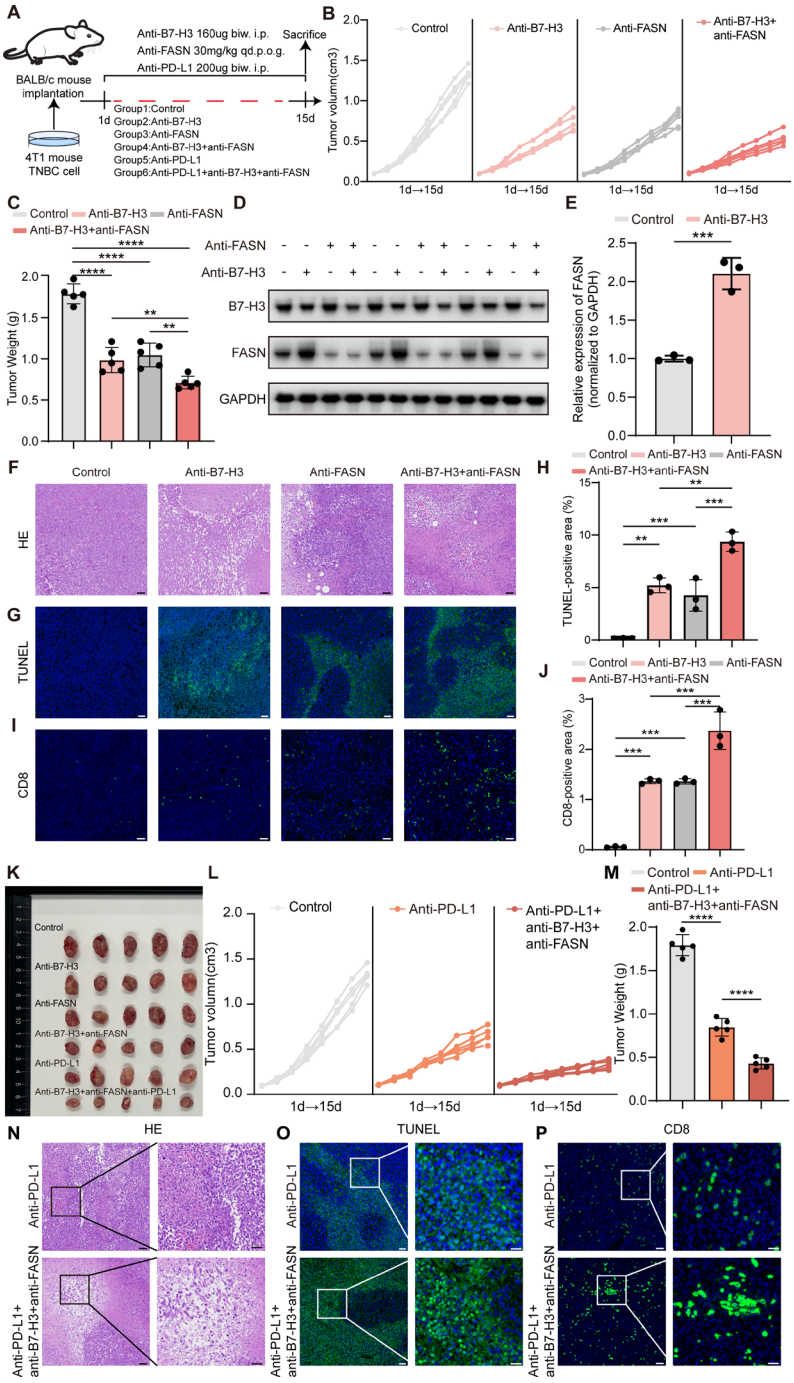

Figure 7 Anti-B7-H3 and anti-FASN combination therapy enhances antitumor activity in vivo. (A) Schematic representation of the treatment protocol using anti-B7-H3, anti-FASN, anti-PD-L1, and combination therapy in BALB/c mice implanted with 4T1 cells (n=5). (B) Tumor growth curves showing tumor volume over time in each treatment group. (C) Comparative analysis of tumor weight among different treatment regimens. Mean±SD is shown (n=5). (D–E) Evaluation of FASN protein expression via Western Blot analysis. Anti-B7-H3 treatment significantly upregulated FASN compared with the control group. Mean±SD is shown (n=3). (F) Representative H&E staining of tumor sections. Scale bars: 50 µm. (G–H) TUNEL staining to assess apoptosis in tumor tissues. The combination therapy induced a higher level of apoptosis, as seen by the increased fluorescence ratio in H. Scale bars: 50 µm. Mean±SD is shown (n=3). (I–J) CD8 immunofluorescence staining to evaluate immune cell infiltration. The combination therapy group showed significantly enhanced $CD8^+$ T cell infiltration, as quantified in panel I. Mean±SD is shown (n=3). (K) Visual pictures showing representative tumor volumes of each treatment group. (L) Tumor growth curves showing tumor volume in control, anti-PD-L1, and combination treatment groups. (M) Effect of anti-PD-L1 and combination therapy on tumor weight in balb/c mice bearing 4T1 cells. Mean±SD is shown (n=5). (N) Representative HE staining of tumor sections. Scale bars: 50 µm (left) and 20 µm (right). (O) TUNEL staining to assess apoptosis in tumor tissues. Scale bars: 50 µm (left) and 20 µm (right). (P) Immunofluorescence staining for $CD8^+$ T Cell Infiltration in Tumor Section. Scale bars: 50 µm (left) and 20 µm (right). Statistical significance was calculated using the Student's t-test for FASN expression and one-way ANOVA with Tukey's multiple-comparison test for other comparisons. **p<0.01, ***p<0.001, ****p<0.0001. ANOVA, analysis of variance.

J Immunother Cancer: first published as 10.1136/jitc-2024-010924 on 12 April 2025. Downloaded from http://jitc.bmj.com/ on May 20, 2025 at Department GEZ-LTA Erasmushogeschool . Protected by copyright, including for uses related to text and data mining, AI training, and similar technologies.

effects, addressing the potential issue of PD-L1 resistance. These results highlight the potential of this approach to enhance immunotherapy efficacy in TNBC.

DISCUSSION

TNBC is characterized by its aggressive behavior, poor differentiation, and rapid progression, which collectively drive its therapeutic resistance and contribute to poor survival outcomes.[34] Current treatment options for TNBC are limited, and the absence of hormone receptors and HER2 expression excludes the use of targeted therapies that have proven effective in other BC subtypes. The growing elucidation of tumor immune evasion mechanisms has driven the evolution of cancer treatment paradigms, transitioning from conventional modalities such as surgery, chemotherapy, and radiotherapy to molecularly targeted therapies.[35] The application of ICIs has ushered in a new era of cancer treatment, offering the potential for durable and effective antitumor immunity.[36 37]

B7-H3, an emerging immune checkpoint molecule, has garnered significant attention for its critical role in regulating tumor immune evasion, modulating immune responses, and influencing tumor behavior.[38 39] A range of B7-H3i is currently being tested in clinical trials to ensure both efficacy and safety in tumor suppression. However, the majority of existing research has concentrated on the epigenetic modulation of B7-H3, leaving a significant gap in understanding the molecular-level effects of B7-H3 inhibition, particularly in the context of TNBC.

Building on our previous research, which proposed a TNBC subtype management strategy based on B7-H3 expression, we extended our investigation through in vitro and in vivo experiments to elucidate its role in TNBC. Our findings confirm that B7-H3 is highly expressed in TNBC, correlating with poor prognosis and increased tumor malignancy. Existing evidence suggests that B7-H3 may play a role in tumor cell metabolism.[40 41] We discovered that inhibiting B7-H3 also led to abnormal activation of FA metabolism, which we identified as a potential factor that could weaken the anticancer efficacy of B7-H3-targeted therapies.

Many cancer cells preferentially rely on increased de novo FA synthesis, whereas normal cells primarily use exogenous FA sources.[42–45] This metabolic reprogramming supports the high proliferative demands of cancer cells.[46 47] The key metabolic multienzyme FASN is responsible for the terminal catalytic step in FA synthesis.[48] Unlike typical anabolic energy storage pathways, tumor-driven lipogenesis mediated by FASN is intricately linked to the progression of several malignancies.[49–53] In our study, we found that B7-H3 knockdown triggered the activation of the Akt signaling pathway, consequently upregulating the transcription factor SREBP1, which in turn drove FASN expression.

These findings suggest that addressing the unintended upregulation of FASN following B7-H3 inhibition could be a promising strategy to enhance the efficacy of B7-H3-targeted therapies. To test this hypothesis, we combined B7-H3 and FASN inhibitors in our final experiments, observing significantly improved antitumor efficacy when both oncogenes were inhibited simultaneously. By uncovering the metabolic vulnerabilities conferred by B7-H3 inhibition, our study lays the groundwork for combination therapies that can maximize therapeutic efficacy.

However, this study has several limitations: While B7-H3 has shown promise as an immunotherapy target in clinical studies, its clinical application remains uncertain. Additionally, whether the FASN activation observed in the lab will manifest similarly in clinical settings requires further validation. The study includes an investigation of B7-H3's effects on proliferation, invasion, and apoptosis but does not assess its metastatic potential in vivo. Furthermore, while the combination therapy successfully recruited $CD8^+$ T cells in animal models, the underlying mechanisms driving this recruitment remain insufficiently elucidated, warranting further investigation.

CONCLUSIONS

Our study establishes B7-H3 as a promising prognostic biomarker and immunotherapy target for TNBC, highlighting its pivotal role in shaping tumor progression and immune evasion. Moreover, our findings unveil a novel link between FA metabolism and the therapeutic modulation of B7-H3, providing fresh insights into enhancing treatment efficacy. We propose a translational strategy to bridge the gap between benchside discoveries of B7-H3 blockade and its anticipated clinical applications, addressing potential challenges in achieving optimal therapeutic outcomes.

Author affiliations
[1]Department of Oncology, Women's Hospital of Jiangnan University, Wuxi School of Medicine, Jiangnan University, Wuxi, Jiangsu, China
[2]Department of Oncology, Wuxi Maternal and Child Health Hospital, Nanjing Medical University, Nanjing, Jiangsu, China
[3]Department of Oncology, The Affiliated Wuxi People's Hospital of Nanjing Medical University, Wuxi People's Hospital, Wuxi Medical Center, Nanjing Medical University, Wuxi, Jiangsu, China
[4]The First Clinical Medicine College, Nanjing Medical University, Nanjing, Jiangsu, China
[5]Department of Breast Surgery, Women's Hospital of Jiangnan University, Wuxi, China

Correction notice This article has been corrected since it was first pubished online. The author Cenzhu Wang was incorrectly listed as Cengzhu Wang.

Contributors YZ, XZ and JM conceived the study, provided clinical expertise, and contributed to data interpretation. YJ was responsible for preparing the figures and drafting the manuscript. ZQ and CW critically revised the initial draft. XN handled literature collection and consultation. YY conducted data visualization. All authors reviewed the manuscript, offered feedback and approved the final version. JM is the guarantor.

Funding The study was supported by the National Natural Science Foundation of China (82472842), Wuxi Double-Hundred Talent Fund Project (BJ2023075), General Program of Wuxi Medical Center of Nanjing Medical University (WMCG202354) and Doctoral Talent Fund of the Affiliated Wuxi People's Hospital of Nanjing Medical University (BSRC202303).

J Immunother Cancer: first published as 10.1136/jitc-2024-010924 on 12 April 2025. Downloaded from http://jitc.bmj.com/ on May 20, 2025 at Department GEZ-LTA Erasmushogeschool . Protected by copyright, including for uses related to text and data mining, AI training, and similar technologies.

Competing interests None declared.

Patient consent for publication Not applicable.

Ethics approval This study involves human participants and ethical approval for the study of TMAs was granted by the Outdo Biotech Clinical Research Ethics Committee. Ethical approval for the single-cell sequencing data was granted by Clinical Research Ethics Committees at Wuxi Maternal and Child Health Care Hospital (Ethics No. 2021-01-0927-28). Participants gave informed consent to participate in the study before taking part.

Provenance and peer review Not commissioned; externally peer reviewed.

Data availability statement Data are available on reasonable request. Not applicable.

Supplemental material This content has been supplied by the author(s). It has not been vetted by BMJ Publishing Group Limited (BMJ) and may not have been peer-reviewed. Any opinions or recommendations discussed are solely those of the author(s) and are not endorsed by BMJ. BMJ disclaims all liability and responsibility arising from any reliance placed on the content. Where the content includes any translated material, BMJ does not warrant the accuracy and reliability of the translations (including but not limited to local regulations, clinical guidelines, terminology, drug names and drug dosages), and is not responsible for any error and/or omissions arising from translation and adaptation or otherwise.

Open access This is an open access article distributed in accordance with the Creative Commons Attribution Non Commercial (CC BY-NC 4.0) license, which permits others to distribute, remix, adapt, build upon this work non-commercially, and license their derivative works on different terms, provided the original work is properly cited, appropriate credit is given, any changes made indicated, and the use is non-commercial. See http://creativecommons.org/licenses/by-nc/4.0/.

ORCID iDs
Jie Mei http://orcid.org/0000-0001-7799-8129
Yan Zhang http://orcid.org/0000-0002-7983-8396

REFERENCES

1 Siegel RL, Miller KD, Wagle NS, *et al*. Cancer statistics, 2023. *CA Cancer J Clin* 2023;73:17–48.
2 Giaquinto AN, Sung H, Newman LA, *et al*. Breast cancer statistics 2024. *CA Cancer J Clin* 2024;74:477–95.
3 Liedtke C, Mazouni C, Hess KR, *et al*. Response to Neoadjuvant Therapy and Long-Term Survival in Patients With Triple-Negative Breast Cancer. *JCO* 2023;41:1809–15.
4 So JY, Ohm J, Lipkowitz S, *et al*. Triple negative breast cancer (TNBC): Non-genetic tumor heterogeneity and immune microenvironment: Emerging treatment options. *Pharmacol Ther* 2022;237:108253.
5 Hua Z, White J, Zhou J. Cancer stem cells in TNBC. *Semin Cancer Biol* 2022;82:26–34.
6 Ye F, Dewanjee S, Li Y, *et al*. Advancements in clinical aspects of targeted therapy and immunotherapy in breast cancer. *Mol Cancer* 2023;22:105.
7 Li Y, Zhang H, Merkher Y, *et al*. Recent advances in therapeutic strategies for triple-negative breast cancer. *J Hematol Oncol* 2022;15:121.
8 Zhang Y, Chen H, Mo H, *et al*. Single-cell analyses reveal key immune cell subsets associated with response to PD-L1 blockade in triple-negative breast cancer. *Cancer Cell* 2021;39:1578–93.
9 Mei J, Cai Y, Zhu H, *et al*. High B7-H3 expression with low PD-L1 expression identifies armored-cold tumors in triple-negative breast cancer. *NPJ Breast Cancer* 2024;10:11.
10 Kanchan RK, Doss D, Khan P, *et al*. To kill a cancer: Targeting the immune inhibitory checkpoint molecule, B7-H3. *Biochim Biophys Acta Rev Cancer* 2022;1877:188783.
11 Wang C, Li Y, Jia L, *et al*. CD276 expression enables squamous cell carcinoma stem cells to evade immune surveillance. *Cell Stem Cell* 2021;28:1597–613.
12 Quintana Á, Peg V, Prat A, *et al*. Immune analysis of lymph nodes in relation to the presence or absence of tumor infiltrating lymphocytes in triple-negative breast cancer. *Eur J Cancer* 2021;148:134–45.
13 Shi W, Wang Y, Zhao Y, *et al*. Immune checkpoint B7-H3 is a therapeutic vulnerability in prostate cancer harboring PTEN and TP53 deficiencies. *Sci Transl Med* 2023;15:eadf6724.
14 Cai D, Li J, Liu D, *et al*. Tumor-expressed B7-H3 mediates the inhibition of antitumor T-cell functions in ovarian cancer insensitive to PD-1 blockade therapy. *Cell Mol Immunol* 2020;17:227–36.
15 Feng Y, Lee J, Yang L, *et al*. Engineering CD276/B7-H3-targeted antibody-drug conjugates with enhanced cancer-eradicating capability. *Cell Rep* 2023;42:113503.
16 Li D, Wang R, Liang T, *et al*. Camel nanobody-based B7-H3 CAR-T cells show high efficacy against large solid tumours. *Nat Commun* 2023;14:5920.
17 Vitanza NA, Wilson AL, Huang W, *et al*. Intraventricular B7-H3 CAR T Cells for Diffuse Intrinsic Pontine Glioma: Preliminary First-in-Human Bioactivity and Safety. *Cancer Discov* 2023;13:114–31.
18 Aggarwal C, Prawira A, Antonia S, *et al*. Dual checkpoint targeting of B7-H3 and PD-1 with enoblituzumab and pembrolizumab in advanced solid tumors: interim results from a multicenter phase I/II trial. *J Immunother Cancer* 2022;10:e004424.
19 Du H, Hirabayashi K, Ahn S, *et al*. Antitumor Responses in the Absence of Toxicity in Solid Tumors by Targeting B7-H3 via Chimeric Antigen Receptor T Cells. *Cancer Cell* 2019;35:221–37.
20 Kramer K, Pandit-Taskar N, Kushner BH, *et al*. Phase 1 study of intraventricular ^{131}I-omburtamab targeting B7H3 (CD276)-expressing CNS malignancies. *J Hematol Oncol* 2022;15:165.
21 Shenderov E, De Marzo AM, Lotan TL, *et al*. Neoadjuvant enoblituzumab in localized prostate cancer: a single-arm, phase 2 trial. *Nat Med* 2023;29:888–97.
22 Rimal R, Desai P, Daware R, *et al*. Cancer-associated fibroblasts: Origin, function, imaging, and therapeutic targeting. *Adv Drug Deliv Rev* 2022;189:114504.
23 van Vlerken-Ysla L, Tyurina YY, Kagan VE, *et al*. Functional states of myeloid cells in cancer. *Cancer Cell* 2023;41:490–504.
24 Cheng N, Bei Y, Song Y, *et al*. B7-H3 augments the pro-angiogenic function of tumor-associated macrophages and acts as a novel adjuvant target for triple-negative breast cancer therapy. *Biochem Pharmacol* 2021;183:114298.
25 Carracedo A, Cantley LC, Pandolfi PP. Cancer metabolism: fatty acid oxidation in the limelight. *Nat Rev Cancer* 2013;13:227–32.
26 Xiao Y, Yu T-J, Xu Y, *et al*. Emerging therapies in cancer metabolism. *Cell Metab* 2023;35:1283–303.
27 Costa GP, Mensurado S, Silva-Santos B. Therapeutic avenues for γδ T cells in cancer. *J Immunother Cancer* 2023;11:e007955.
28 Sebestyen Z, Prinz I, Déchanet-Merville J, *et al*. Translating gammadelta (γδ) T cells and their receptors into cancer cell therapies. *Nat Rev Drug Discov* 2020;19:169–84.
29 Wu Y-C, Yan Q, Yue S-Q, *et al*. NUP85 alleviates lipid metabolism and inflammation by regulating PI3K/AKT signaling pathway in nonalcoholic fatty liver disease. *Int J Biol Sci* 2024;20:2219–35.
30 Yi J, Zhu J, Wu J, *et al*. Oncogenic activation of PI3K-AKT-mTOR signaling suppresses ferroptosis via SREBP-mediated lipogenesis. *Proc Natl Acad Sci U S A* 2020;117:31189–97.
31 Feng D, Pu D, Ren J, *et al*. CD8$^+$ T-cell exhaustion: Impediment to triple-negative breast cancer (TNBC) immunotherapy. *Biochim Biophys Acta Rev Cancer* 2024;1879:189193.
32 Cortes J, Cescon DW, Rugo HS, *et al*. Pembrolizumab plus chemotherapy versus placebo plus chemotherapy for previously untreated locally recurrent inoperable or metastatic triple-negative breast cancer (KEYNOTE-355): a randomised, placebo-controlled, double-blind, phase 3 clinical trial. *Lancet* 2020;396:1817–28.
33 Schmid P, Cortes J, Dent R, *et al*. Event-free Survival with Pembrolizumab in Early Triple-Negative Breast Cancer. *N Engl J Med* 2022;386:556–67.
34 Derakhshan F, Reis-Filho JS. Pathogenesis of Triple-Negative Breast Cancer. *Annu Rev Pathol* 2022;17:181–204.
35 Ribas A, Wolchok JD. Cancer immunotherapy using checkpoint blockade. *Science* 2018;359:1350–5.
36 Holder AM, Dedeilia A, Sierra-Davidson K, *et al*. Defining clinically useful biomarkers of immune checkpoint inhibitors in solid tumours. *Nat Rev Cancer* 2024;24:498–512.
37 Waldman AD, Fritz JM, Lenardo MJ. A guide to cancer immunotherapy: from T cell basic science to clinical practice. *Nat Rev Immunol* 2020;20:651–68.
38 Zhao B, Li H, Xia Y, *et al*. Immune checkpoint of B7-H3 in cancer: from immunology to clinical immunotherapy. *J Hematol Oncol* 2022;15:153.
39 Kontos F, Michelakos T, Kurokawa T, *et al*. B7-H3: An Attractive Target for Antibody-based Immunotherapy. *Clin Cancer Res* 2021;27:1227–35.
40 Kotewitsch M, Heimer M, Schmitz B, *et al*. Non-coding RNAs in exercise immunology: A systematic review. *J Sport Health Sci* 2024;13:311–38.
41 Pulanco MC, Madsen AT, Tanwar A, *et al*. Recent advancements in the B7/CD28 immune checkpoint families: new biology and clinical therapeutic strategies. *Cell Mol Immunol* 2023;20:694–713.

J Immunother Cancer: first published as 10.1136/jitc-2024-010924 on 12 April 2025. Downloaded from http://jitc.bmj.com/ on May 20, 2025 at Department GEZ-LTA Erasmushogeschool . Protected by copyright, including for uses related to text and data mining, AI training, and similar technologies.

42 Bacci M, Lorito N, Smiriglia A, *et al*. Fat and Furious: Lipid Metabolism in Antitumoral Therapy Response and Resistance. *Trends Cancer* 2021;7:198–213.
43 Bar-Peled L, Kory N. Principles and functions of metabolic compartmentalization. *Nat Metab* 2022;4:1232–44.
44 Grabner GF, Xie H, Schweiger M, *et al*. Lipolysis: cellular mechanisms for lipid mobilization from fat stores. *Nat Metab* 2021;3:1445–65.
45 Broadfield LA, Pane AA, Talebi A, *et al*. Lipid metabolism in cancer: New perspectives and emerging mechanisms. *Dev Cell* 2021;56:1363–93.
46 Snaebjornsson MT, Janaki-Raman S, Schulze A. Greasing the Wheels of the Cancer Machine: The Role of Lipid Metabolism in Cancer. *Cell Metab* 2020;31:62–76.
47 Bian X, Liu R, Meng Y, *et al*. Lipid metabolism and cancer. *J Exp Med* 2021;218:e20201606.
48 Xiao Y, Yang Y, Xiong H, *et al*. The implications of FASN in immune cell biology and related diseases. *Cell Death Dis* 2024;15:88.
49 Du Q, Liu P, Zhang C, *et al*. FASN promotes lymph node metastasis in cervical cancer via cholesterol reprogramming and lymphangiogenesis. *Cell Death Dis* 2022;13:488.
50 Bartolacci C, Andreani C, Vale G, *et al*. Targeting de novo lipogenesis and the Lands cycle induces ferroptosis in KRAS-mutant lung cancer. *Nat Commun* 2022;13:4327.
51 Ferraro GB, Ali A, Luengo A, *et al*. FATTY ACID SYNTHESIS IS REQUIRED FOR BREAST CANCER BRAIN METASTASIS. *Nat Cancer* 2021;2:414–28.
52 Wei W, Qin B, Wen W, *et al*. FBXW7β loss-of-function enhances FASN-mediated lipogenesis and promotes colorectal cancer growth. *Signal Transduct Target Ther* 2023;8:187.
53 Liu B, Zhao X, Zhang S, *et al*. Targeting ZDHHC21/FASN axis for the treatment of diffuse large B-cell lymphoma. *Leukemia* 2024;38:351–64.

J Immunother Cancer: first published as 10.1136/jitc-2024-010924 on 12 April 2025. Downloaded from http://jitc.bmj.com/ on May 20, 2025 at Department GEZ-LTA Erasmushogeschool . Protected by copyright, including for uses related to text and data mining, AI training, and similar technologies.